Near-infrared light absorption and scattering based on a mono-layer of gold nanoparticles

R. Soltanmoradi   Optics and Photonics, School of Information and Communication Technology, KTH – Royal Institute of Technology, Isafjordsgatan 22, Kista 164 40, Sweden

Q. Wang   ACREO Swedish ICT AB, Isafjordsgatan 22, Kista 164 40, Sweden

M. Qiu   State Key Laboratory of Modern Optical Instrumentation, Department of Optical Engineering, Zhejiang University, 310027 Hangzhou, China
            Optics and Photonics, School of Information and Communication Technology, KTH – Royal Institute of Technology, Isafjordsgatan 22, Kista 164 40, Sweden

S. Popov   Optics and Photonics, School of Information and Communication Technology, KTH – Royal Institute of Technology, Isafjordsgatan 22, Kista 164 40, Sweden

M. Yan   Optics and Photonics, School of Information and Communication Technology, KTH – Royal Institute
miya@kth.se   of Technology, Isafjordsgatan 22, Kista 164 40, Sweden

We report fabrication and characterization of large-area ultrathin near-infrared light absorbers and scatterers based on a mono-layer of gold nanoparticles laying on top of a dielectric spacer and an aluminum reflector. The nanoparticles are formed through thermal annealing of an evaporated continuous gold film. Through optimization of initial gold-film thickness, spacer thickness, as well as annealing temperature we obtained samples that exhibit very low (~2%) broadband specular reflectance at near-infrared (NIR) wavelength range. By considering also diffuse reflection, we identify that the low specular reflectance can be due to either relatively high light absorption (~70%) or high light scattering (over 60%), with the latter achieved for samples having relatively sparse gold nanoparticles. Both strong absorption and scattering of NIR light are not inherent properties of the bulk materials used for fabricating the samples. Such composite optical surfaces can potentially be integrated to solar-energy harvesting and LED devices.
[DOI: http://dx.doi.org/10.2971/jeos.2015.15031]

Keywords: Light absorber, light scattering, optical thin films, metamaterial surface

1 INTRODUCTION

Optical properties of metals can be strongly altered through structuring at nanoscale. Lateral patterning of noble metals, such as gold and silver, in combination with multilayered substrate (or structuring at vertical direction) can produce perfect absorbers for visible [1]–[3], near-infrared (NIR) [4, 5], infrared and terahertz [6]–[8] light, and even radio waves [9]. Two decent reviews of recent research activities on electromagnetic wave absorbers can be found in [10, 11]. Applications of such light absorption can be multiple-faceted, ranging from photothermal tuning of nanophotonic devices [12] to solar-energy harvesting and enhanced IR detectors or bolometers. One can also, according to Kirchoff's law, devise structures with tailored thermal emission characteristics at desired spectral range by optimizing the structures' light absorption properties [6, 13]. Besides absorption, it is also known that plasmonic nanostructures can serve as efficient antennas at optical frequencies, as evidenced by recent studies on optical Yagi-Uda antenna [14], superscatterers [15] and phase-discontinuous metamaterial surfaces [16].

A common architecture for achieving electromagnetic wave absorption with metal-dielectric materials is based on the so-

called Salibury screen geometry, where three basic layers are, from top to bottom, a thin metal layer (sometimes nano- or micro-nanostructured), a lossless dielectric spacer layer, and a metal reflector or ground plane. Owing to its structural simplicity and effectiveness, this architecture has been the basis of many recent works on electromagnetic wave absorbers [1]–[9]. Majority of the previous work on absorbers are relying on regularly patterned nanostructures, which are usually done with some lithography technique [1]–[9]. Especially, for absorbers at visible or NIR wavelengths, the required structural feature size is usually at sub-micrometer scale. For that purpose, electron-beam lithography (EBL) technique is generally deployed for obtaining necessary patterning resolution. Unfortunately EBL can't efficiently produce large-area samples, which is inherently limited by its scanning-exposure procedure. Some techniques such as nanoimprint technology [17] and colloidal lithography [18] can to a certain degree circumvent this fabrication bottleneck. It was well known that the peculiar dewetting property of heated gold or silver thin films on a dielectric substrate can induce breaking and agglomeration of the metal material, forming well-separated nano-islands. Although the sizes of islands can be random, its average size

can be controlled through changing initial metal film thickness, deposition conditions, as well as annealing temperature and duration, etc. A mono-layer of gold or silver nanoparticles derived from this mold- and mask-free technique therefore can nevertheless fulfill requirements of certain applications. In fact, the potential of achieving broadband optical responses by the resulted random particles can be advantageous for some applications. One example is the recently reported visible light absorber which, thanks to a mono-layer of random gold nanoparticles, absorbs almost the whole visible-light spectrum [19].

The broadband visible light absorption achieved by localized plasmonic responses from a mono-layer of gold nanoparticles as well as electromagnetic coupling between the particles and the metal reflector [19] can be treated as the short-wavelength extreme case of light absorber based on the Salibury-screen geometry. One can potentially extend such strong light response into NIR or probably IR spectral range by proper controlling formation of gold nanoparticles through various fabrication parameters, predominately through tailoring as-deposited gold-film thickness and annealing temperature. In the current study, we start with a similar initial geometry including a bottom metal reflector, a dielectric spacer, and a top gold-nanoparticle layer, with the latter two layers' thicknesses increased compared to those in [19]; thermal annealing at various temperatures is then carried out to study NIR responses of the obtained samples. We observed that such a sample can possess a strong extinction ($1-R$, where R is specular reflectance) band centered just over 1 μm wavelength with a full-width at half-maximum of approximately 1 μm. Depending on morphology of the annealed gold nanoparticles, the strong extinction can be attributed dominantly to either strong light absorption or strong light scattering (i.e. diffuse reflection). By closely examining the particle-size distribution, we identify that strong diffuse light reflection is achieved when gold nanoparticles have a relatively sparse distribution. Strong diffuse light reflection was not observed in previous studies based on structures sharing a similar geometry (with either periodic or aperiodic metal nanoparticles) [1]–[5], [17]–[19]. Such large-area and cost-effective metamaterial surfaces can be potentially used in optoelectronic applications: strong light absorption (or minimum total reflection) can be used for e.g. solar thermal collectors; strong diffuse light reflection (with minimum loss) can be used for reflection-plane design of photovoltaic cells and LED devices.

2 SAMPLE GEOMETRY AND FABRICATION

Before thermal annealing, the samples have three continuous layers deposited on a silicon wafer substrate. Refer to the schematic diagram shown in Figure 1(a), the top layer is a thin gold layer; the middle layer is a dielectric spacer, of material Al_2O_3 in this work; the bottom layer is aluminum of 100 nm thick, serving as an optical reflector throughout visible to IR wavelengths. Aluminum is used in this work for reflector since at NIR wavelengths its reflectance is comparable a gold mirror and it is definitely more economical; while in [19] gold was used for reflector because there the native absorptivity of gold at blue wavelength is harnessed to achieve
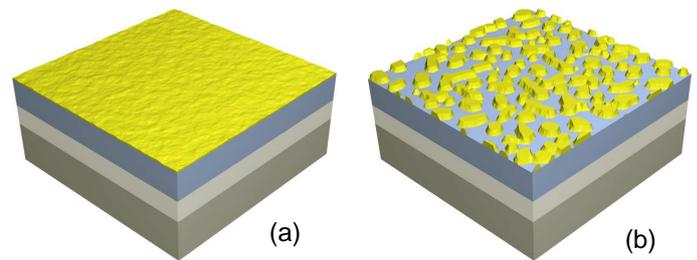

FIG. 1 The schematic 3D image of the multilayer structure: (a) before thermal annealing; (b) after annealing. From top to bottom: thin gold layer (yellow), dielectric spacer (blue), aluminum reflector (light gray), and silicon substrate (dark gray).

better light absorption across the whole visible range. In some other studies [5, 12], gold bottom reflector was used merely for the convenience of material deposition (one uses two material sources instead of three). The aluminum layer is deposited using an electron-beam evaporation system. Atomic layer deposition (ALD) technique is then used to deposit the Al_2O_3 layer. The advantage of using ALD is that it has precise control of the deposited layer thickness with a sub-nanometer accuracy. We have fabricated a range of samples with different Al_2O_3 thicknesses, ranging from 80 to 194 nm. Finally, the top gold layer is deposited, again with an electron-beam evaporation system. For optimization purpose, for each fixed spacer thickness, we have prepared three samples with top-gold layer thicknesses at nominally 15, 21, and 27 nm. The deposition pressure of the gold layer is 5×10^{-6} mBar and the rate of deposition is 2 Å/s.

The samples are then cleaved into smaller pieces of size around 2×2 cm^2. Thermal annealing is done with a resistively heated oven (Nabertherm Model L3) in atmospheric environment. To investigate the effect of annealing temperature, the targeted temperatures were set at values ranging from 350°C to 450°C. The temperature ramps up in about 30 minutes. After further 20 minutes, the oven was turned off. During the 20 minutes, temperature inside overshoots by about 70°C. After the oven is turned off, the chamber temperature decreases to 125°C in about 50 minutes; then the samples are taken out.

It is well known that, under extended exposure to heating (even well under the melting temperature of bulk gold), a thin gold film can undergo softening. The combined effects of surface tension and crystallization gradually cause breakage of the film. As a result, a monolayer of gold nanoparticles can be formed after an extended period of thermal annealing. The phenomenon happens often when the gold layer is on an oxide surface. An illustration of an annealed sample is presented in Figure 1(b), where the gold particles can have sizes from tens of nanometers to hundreds of nanometers.

The transformation of a 21 nm-thick gold film, on top of a Al_2O_3 film (110 nm thick), after being annealed under various temperatures is vividly shown by the scanning-electron microscope (SEM) images in Figure 2(a)–(c). Note that in our experiments we have tried to avoid any uncertainty during fabrication and thermal annealing processes. In the current case, all three samples used for thermal annealing are from the same bigger wafer piece, ensuring that their geometries are identical. In other cases, if samples to be compared share
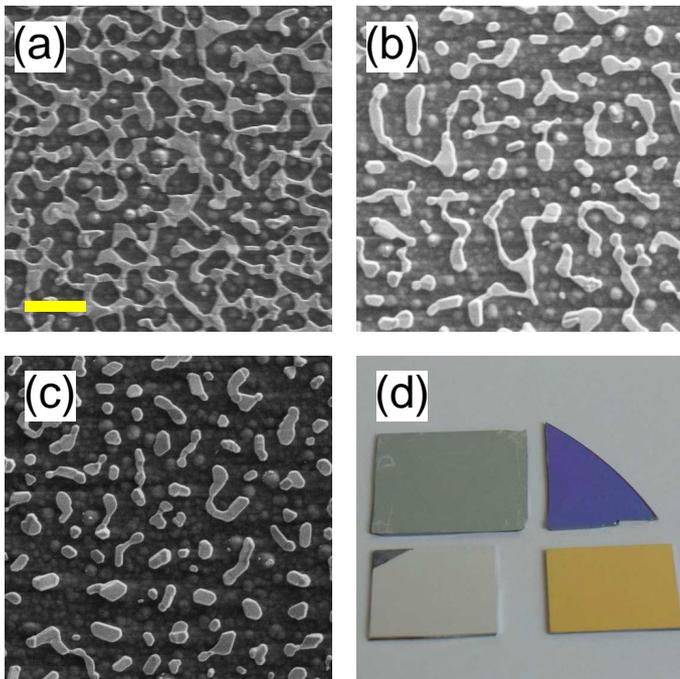
FIG. 2 Effect of annealing temperature to a 21 nm-thick gold thin film, deposited on top of a 110 nm thick Al_2O_3 layer. (a) Annealing temperature 350°C; (b) 400°C; and (c) 450°C. Scale bar represents 1 μm. (d) Top-left: photograph of the sample after thermal annealing at 450°C (corresponding SEM image shown in (c)); top-right: the sample before thermal annealing; bottom-left: aluminum film; bottom-right: gold film.

the same top gold layer, their top gold layer is deposited in the same deposition process. And similarly, if different samples are to be annealed at the same temperature, one single thermal annealing process is used. From Figure 2, one sees that metal islands start to take form when the temperature is set at 350°C (Figure 2(a)); but still the film as a whole is, to a large degree, percolated. At 400°C (Figure 2(b)), metal islands are mostly separated. Annealing at 450°C gives clear separated gold nanoparticles (Figure 2(c)). We also tried sample annealing at a higher temperature (500°C), which results in smaller particles primarily owing to further agglomeration of gold atoms. We notice that samples with well-separated gold nanoparticles give rise to better light extinction (absorption plus scattering). At the same time we wish to have larger particles in order to achieve light extinction at NIR or even longer wavelengths. Therefore in this study, we concentrate on samples annealed under temperature 450°C.

The visual appearance of one sample (top gold layer of thickness 21 nm, and spacer 110 nm), before and after thermal annealing (450°C), as compared to aluminum and gold films, are shown in Figure 2(d). The drastic change of the visible color is due to structural change of the top gold film, confirming the strong optical response resulted from a mono-layer of gold nanoparticles as well as its electromagnetic coupling with the bottom aluminum reflector.

In Figures 3(a)–(c), we show three annealed samples based on different initial gold-film thicknesses (15, 21, 27 nm). Thermal annealing for three samples was carried out in a single annealing process under 450°C. It is clear that all samples have well-separated nanoparticles, and evidently the particles are much smaller for the sample initially prepared with a thin gold film.

To gain more quantitative knowledge regarding the particle sizes, we used an image-processing tool to extract the statistic size-distributions of particles based on high-resolution SEM images. The results are shown in Figures 3(d)–(f). The sample area concerned is about 730 μm^2 for all three samples, and particle numbers counted are from 2000 to 5500. We convert all particles to circular shapes, and use their diameters to characterize their sizes. We should here stress that, in order to rule out fabrication or annealing uncertainty, we have tried to use batch processes to treat samples whenever possible during material-deposition and annealing procedures. Indeed, we observed that particle size distributions as well as optical reflection spectra are similar for samples resulted from repeated fabrications under identical process settings. Furthermore, we confirmed that the optical measurements at different spots (a few millimeters in size) of a sample give rise to almost identical reflection curves.

The sample corresponding to an initial gold thickness of 15 nm (Figure 3(d)) has two dominant peaks in its particle-size distribution. The first peak is around 50 nm; such particles lead to localized plasmon resonances at visible wavelengths [19]. The other peak around 150 nm is more relevant to the current work; particles at such a size can lead to strong light extinction at NIR wavelengths [5]. The second sample with initial gold film thickness of 21 nm (Figure 3(e)) has also two peaks in size distribution, with the first appearing similarly around 50 nm. The second peak shifts to 300 nm, significantly larger than those in the first sample. The larger particles, as will be shown in the following section, help to achieve light extinction at longer wavelengths. Different from first two samples, the sample with initial gold-film thickness of 27 nm (Figure 3(f)) has a single particle-size distribution peak. And even more intriguingly, the peak is centered around 265 nm, slightly smaller than the second peak found in Figure 3(e). A comparison of Figure 3(d)–(f) tells that the particles-size distribution is not simply scalable based on the initial gold-film thickness, given the same annealing temperature and duration. Nevertheless, there are much more large particles for the third sample compared to the second sample per unit sample area. The SEM images in Figures 3(a)–(c) were at the same time analyzed to obtain the filling ratios of the gold nanoparticles, which are respectively at 0.33, 0.24, and 0.31. One can henceforth estimate the final particle heights, which are at 45.5 nm, 87.5 nm, and 87.1 nm respectively, assuming all particles are of equal height. Interestingly, the two last samples have very similar particle heights. Whether or not samples with different initial gold-film thicknesses exhibit certain type of saturation on their particle size or height (or even both) under a fixed annealing process is not completely known, and deserves further investigation.

3 OPTICAL CHARACTERIZATION: SPECULAR REFLECTION

Owing to their randomness in particle shapes and sizes, the samples are difficult to be modeled through a numerical approach. The larger average particle sizes compared to the samples studied in [19] further prevent a full 3D numerical simulation of their light reflection properties. As dis-
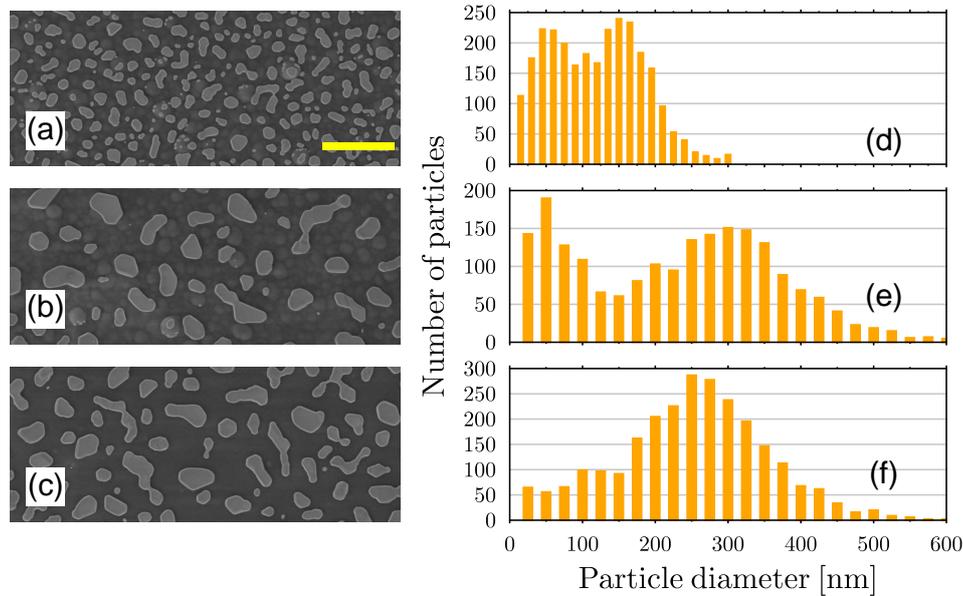
FIG. 3 Effect of initial gold-film thickness on the annealing result. The initial gold-film thicknesses are at (a) 15 nm; (b) 21 nm; (c) 27 nm. The samples have the same spacer thickness of 110 nm. Scale bar (common for three panels): 1 μm. The particle-size distributions of samples in (a)–(c) are shown in (d)–(f), respectively. Particles are converted to circular shapes, whose diameters are used to characterize their size. For all three cases, sample area examined is about 730 μm².
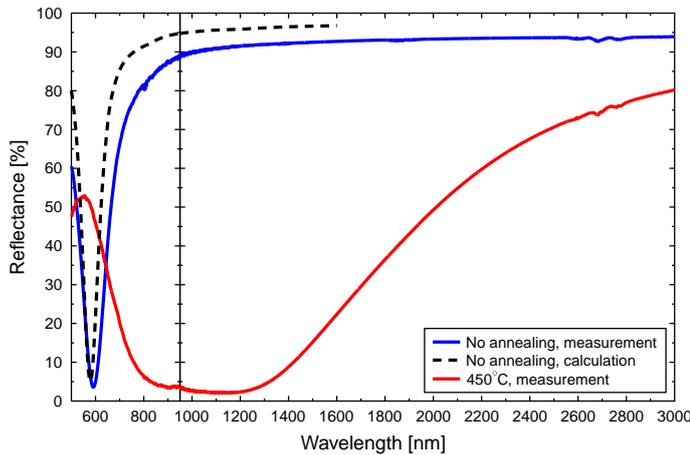

FIG. 4 Specular reflectance spectra of the sample with 21 nm top gold layer and 110 nm spacer before and after annealing (450°C). The reflectance spectrum of the idealized multilayer structure corresponding to the as-deposited sample is calculated and shown in dashed black line.

trometer and a supercontinuum light source (SuperK COM-PACT from NKT Photonics A/s). For the wavelength range between 950 nm and 3 μm, we rely on a Fourier-transform IR (FTIR) spectroscopy tool (VERTEX 70v, Bruker Corporation) with an NIR light source. For the latter system, a Potassium Bromide (KBr) broadband beam splitter, and an ultra-wide-range room-temperature DLaTGS detector are deployed to obtain the reflectance spectra. For each sample, its overall reflectance spectrum is obtained by joining two measured curves with the two systems. At 950 nm wavelength, two sections of the curves, measured with two setups, are susceptible to some mismatch (<5%). This is expected, because the particular wavelength is at the detection limits of both measurement systems. The incidence angle is consistently fixed at 10 degrees on both setups. It was noticed that the specular reflectance of the samples after annealing is not sensitive to incident angle, especially when the incidence angle is small; the same was observed in [19]. Diffuse reflectance will be discussed in the following section of the paper.

The measured reflectance spectra of the sample with 21 nm top gold layer and 110 nm spacer before and after thermal annealing at 450°C are shown in Figure 4. Before annealing, the sample exhibits a strong absorption band close to 600 nm wavelength, which explains why the sample has a cold (bluish) appearance (Figure 2(d)). The absorption band is due to the Fabry-Pérot resonance sustained by the top semi-transparent gold film and the bottom aluminum reflector [23]. After annealing, absorption at visible spectrum decreases due to degradation of the top gold film as a mirror at visible wavelength; instead, a broadband dip emerge in the reflectance spectrum. This dip, as to be revealed in the next section, is attributed to strong light scattering by the nanostructure. The reflection dip is centered around 1.2 μm wavelength and has a bandwidth of approximately 1 μm, indicating broadband optical response of the mono-layer of gold nanoparticles obtained.

cussed in [19], light absorption is achieved through mainly three mechanisms: dipole and multipole resonances (sometimes coupled) in the gold nanoparticles, coupling of incident light to surface-plasmon polariton waves guided by the reflector-spacer interface with gold particles acting as a random grating, and the so-called magnetic-dipole resonances caused by anti-parallel coupling between the dipolar particle resonances and their image dipoles in the bottom reflector [5]. We also note that electromagnetic coupling between a nanoparticle and a metallic surface has been studied in several seminar works [20]–[22].

We start optical characterization of the samples by examining their specular reflectance. It was observed that the main dip in the reflection spectra of all samples crosses 1 μm wavelength. Owing to limitations of detection range of detectors used, optical characterization has to be carried out with two measurement setups. For the wavelength range of 500–950 nm, we use a home-made setup which has a Si-based spec-
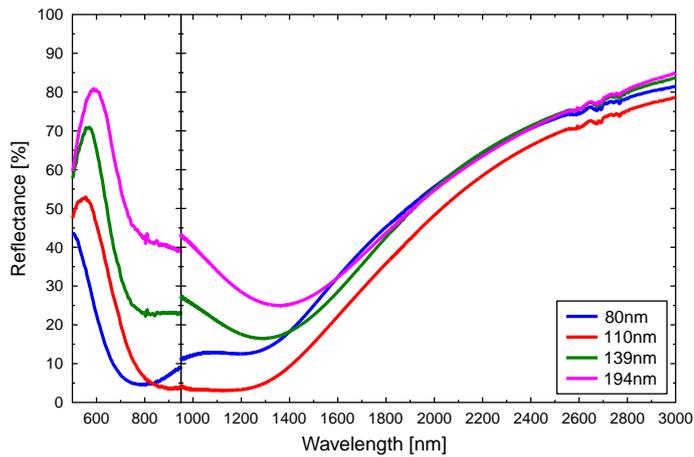
FIG. 5 Effect of spacer thickness on the sample's specular reflectance. All the samples have a 21 nm-thick top gold layer, and are annealed under 450°C.
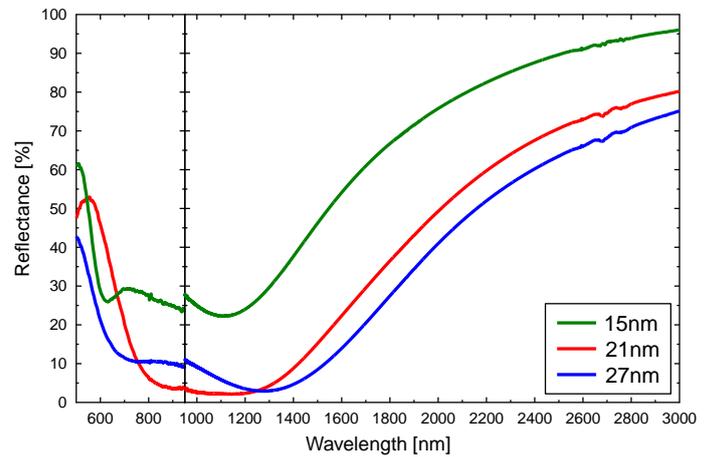

FIG. 6 Effect of the top gold layer thickness (as deposited) on the specular reflection spectra of the annealed samples. All three samples have a common spacer thickness of 110 nm and are annealed at 450°C.

We also calculated the reflectance spectrum of the sample before annealing based on a transfer-matrix method [23], assuming all idealized smooth layers. The optical constant of gold, Al_2O_3, Al are from references [24]–[26], respectively; silicon substrate is neglected in the calculation. Refer to Figure 4, the calculated curve agree nicely with the measured one, except that the absorption band appears narrower in the calculated spectrum (higher quality factor of the Fabry-Pérot cavity). The deteriorated quality factor should be due to surface roughness of the deposited thin films, as schematically shown by Figure 1(a).

Both the spacer thickness and the sizes of gold nanoparticles in the top layer are identified as key factors for the composite's reflection characteristics. The latter, i.e. the sizes of gold nanoparticles, can, to a certain extent, be controlled through the thickness of deposited gold film, as revealed in Figure 3. In the following we show respectively the effect of the spacer thickness and that of the deposited gold film thickness.

The effect of Al_2O_3 spacer thickness on the final sample's specular reflection spectrum is presented in Figure 5. Four samples of spacer thicknesses 80, 110, 139, and 194 nm respectively, all with a 21 nm-thick gold film, were annealed at 450°C. In general, one can see that the main reflectance dip between 600–3000 nm wavelength range is from superposition of two dips; one is near 800 nm, and the other is around 1300 nm. These two dips should be correspondingly contributed by two dominant groups of particles shown in the statistical size distribution in Figure 3(e). This is consistent with the observation [19] that particles with sizes around 30 nm give rise to strong light absorption around 700 nm wavelength. A comparison of the curves shows that when the spacer thickness increases, the spectrum exhibits a slight red shift. Note that the red shift can be obscured by the vertical shifts of the curves. The valley of the reflection dip first decreases, reaching to ∼2% at 110 nm spacer thickness, and then increases at thicker spacers.

The effect of the as-deposited gold film thickness on the final sample's specular reflection spectrum is demonstrated in Figure 6. Three samples, with top gold film thicknesses of 15, 21 and 27 nm and the same spacer thickness of 110 nm, were

simultaneously annealed at 450°C. For the first two samples (gold-film thicknesses of 15 and 21 nm), a thicker gold film leads to a combination of broadening and red shift of the reflection dip. It is in accordance with their size distributions shown in Figure 3. Compare reflectance spectra of the second and third samples (gold-film thicknesses of 21 and 27 nm, respectively); there is no obvious spectral shift, again consistent with the their particle-size distributions in Figure 3. The third sample exhibits a broader spectral response, which might be related to its higher particle density. It is known that closely packed metal particles (aggregates) can lead to red shift of their collective resonance.

4 OPTICAL CHARACTERIZATION: DIFFUSE REFLECTION

Compared to the absorbers presented in [19], in which the top-layer gold particles have an average size well below 50 nm, the samples presented here have particle sizes of a few hundreds of nanometers. This suggests that, besides absorption, light can be scattered by the particles, giving rise to diffuse reflection of the samples. This can especially be true for samples obtained from an initial gold-film thickness of 21 nm, since their particle density is the lowest (or the largest particle-to-particle spacing). The direct consequence is that, the dips of the specular reflectance curves shown in Figures 4 to 6 might not be solely due to absorption of the samples, but also due to diffuse reflection of the incident beam to random directions. To quantify the contribution of diffuse reflection, we use an integration sphere to measure the total reflectance of the samples, which is the summation of diffuse and specular reflections.

The first sample examined has initially a top gold film of 27 nm thick, and a spacer of 110 nm thick (whose specular reflectance was shown as the blue curve in Figure 6). The incident angle is 8 degrees as limited by the setups. The total reflectance is presented in Figure 7. The curve for spectral range above 1 µm is noticeably noisier owing to weak signal reaching the detector. The specular reflectance is also superimposed in the figure. A subtraction of the curves tells that the diffuse reflection (black line in Figure 7) can amount up to 30%, with
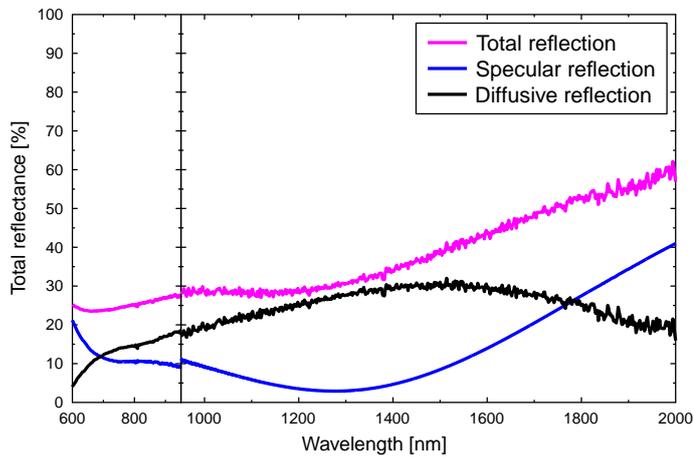
FIG. 7 Total, specular, and diffuse reflection spectra of the sample which originally has 27 nm-thick gold film and a spacer thickness of 110 nm. The sample is annealed at 450°C. The specular reflection curve was also shown Figure 6.
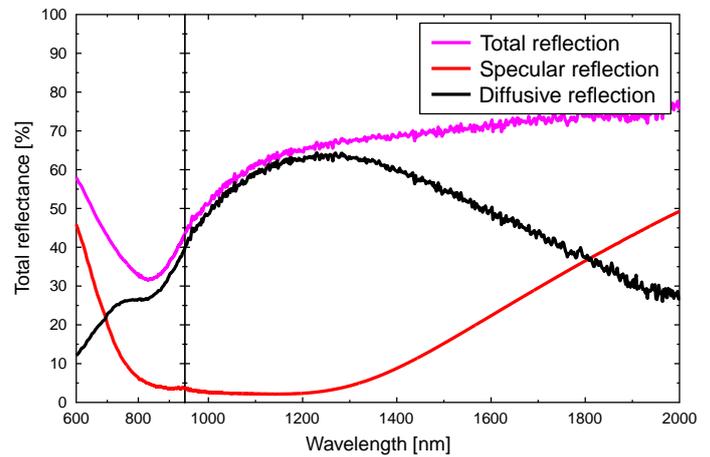

FIG. 8 Total, specular, and diffuse reflection of the sample which originally has 21 nm-thick gold film and a spacer thickness of 110 nm. The sample is annealed at 450°C. The specular reflection curve also appeared in Figures 5 and 6.

a maximum around 1.5 μm. Interestingly, it is observed that the diffuse reflection at shorter wavelengths can be significantly smaller. The scattering of incident light should be due to that the nanostructured surface can no longer be approximated as a flat surface at the concerned wavelength range; contributing factors can be either large particle size or/and large particle-to-particle spacing. Despite the existence of diffuse reflection, the overall optical reflectance of the sample has been decreased by over 60% through just a thermal annealing. The absolute NIR light absorption by the sample is ∼70%; and the absorption response is of broadband nature.

Samples resulted from thermal annealing of a 21 nm-thick gold film differs significantly from those based on a 27 nm-thick gold film. One example is given in Figure 8. The sample originally has a 21 nm-thick as-deposited top gold, and a spacer thickness of 110 nm (i.e. red curve in Figure 6). Annealing temperature is 450°C. The specular reflection curve was shown before in Figures 5 and 6. The total and hence the diffuse reflection curves are presented in Figure 8. From the figure, one sees that the maximum diffuse reflection is 64%. From the total reflection spectrum, one knows that absorption by the composite film is at a maximum value of 68% around 850 nm wavelength, and decreases gradually to around 30% across 1–2 μm wavelength range. The measured large diffuse reflectance at NIR wavelength range should be contributed by its low particle density or equivalently large particle-to-particle spacing of the sample (refer to Figure 3).

5 CONCLUSION

We demonstrated in this work that a mono-layer of gold nanoparticles, assisted by a dielectric spacer and a substrate mirror, can exhibit very dynamic optical response in terms of optical reflection and absorption characteristics. In particular, we used a single thermal annealing step with different annealing temperatures to transform a thin as-deposited gold nanofilm into particles with sizes in the range of hundreds of nanometers. Depending on exact spacer thickness, initial gold film thickness, and annealing temperature, we have realized samples that exhibit either broadband light absorption (>70% from 600 to 1300 nm in measured spectral range) or broad-

band diffuse reflection (maximum 64%, with >50% achieved between 1000 and 1600 nm in free-space wavelength). High diffuse NIR light reflection can be achieved by samples with a relatively sparse distribution of gold nanoparticles. We believe that these values can be further improved, at the studied NIR wavelength range or even beyond, through optimization in film-deposition parameters as well as annealing conditions. Both absorption and scattering of light are not inherent with the bulk metals (gold and aluminum) and dielectric material (alumina) used at the concerned wavelength range. Strong light absorption can be utilized for solar energy harvesting, especially in solar thermal collectors; and strong light scattering can be potentially used for designing, e.g. backplane of conventional photovoltaic panels, as well as in LEDs for converting a directional beam to diffusive light. The lithography-free technique of forming the mono-layer of gold nanoparticles promises feasibility of low-cost and large-area device fabrications.

6 ACKNOWLEDGEMENTS

References

[1] K. Aydin, V. E. Ferry, R.M. Briggs, and H. A. Atwater, "Broadband polarization-independent resonant light absorption using ultrathin plasmonic super absorbers," Nat. Commun. **2**, 1–7 (2011).

[2] M. K. Hedayati, M. Javaherirahim, B. Mozooni, R. Abdelaziz, A. Tavassolizadeh, V. S. K. Chakravadhanula, V. Zaporojtchenko, et al., "Design of a perfect black absorber at visible frequencies using plasmonic metamaterials," Adv. Mater. **23**, 5410–5414 (2011).

[3] A. Moreau, C. Ciracì, J. J. Mock, R. T. Hill, Q. Wang, B. J. Wiley, A. Chilkoti, et al., "Controlled-reflectance surfaces with film-coupled colloidal nanoantennas," Nature **492**, 86–89 (2012).

[4] N. Liu, M. Mesch, T. Weiss, M. Hentschel, and H. Giessen, "Infrared perfect absorber and its application as plasmonic sensor," Nano Lett. **10**, 2342–2348 (2010).

[5] J. Hao, J. Wang, X. Liu, W. J. Padilla, L. Zhou, and M. Qiu, "High performance optical absorber based on a plasmonic metamaterial," Appl. Phys. Lett. **96**, 251104 (2010).

[6] X. Liu, T. Tyler, T. Starr, A. F. Starr, N.M. Jokerst, and W.J. Padilla, "Taming the blackbody with infrared metamaterials as selective thermal emitters," Phys. Rev. Lett. **107**, 045901 (2011).

[7] S. Ogawa, D. Fujisawa, H. Hata, M. Uetsuki, K. Misaki, and M. Kimata, "Mushroom plasmonic metamaterial infrared absorbers," Appl. Phys. Lett. **106**, 0411105 (2015).

[8] H. Tao, N. I. Landy, C. M. Bingham, X. Zhang, R. D. Averitt, and W. J. Padilla, "A metamaterial absorber for the terahertz regime: design, fabrication and characterization," Opt. Express **16**, 7181–7188 (2008).

[9] N. I. Landy, S. Sajuyigbe, J. J. Mock, D. R. Smith, and W. J. Padilla, "Perfect metamaterial absorber," Phys. Rev. Lett. **100**, 207402 (2008).

[10] C. M. Watts, X. Liu, and W. J. Padilla, "Metamaterial electromagnetic wave absorbers," Adv. Mater. **24**, OP98–OP120 (2012).

[11] M. K. Hedayati, F. Faupel, and M. Elbahri, "Review of plasmonic nano composite metamaterial absorber," Materials **7**, 1221–1248 (2014).

[12] Y. Shi, X. Chen, F. Lou, Y. Chen, M. Yan, L. Wosinski, and M. Qiu, "All-optical switching of silicon disk resonator based on photothermal effect in metal-insulator-metal absorber," Opt. Lett. **39**, 4431–4434 (2014).

[13] J. A. Schuller, T. Taubner, M. L. Brongersma, "Optical antenna thermal emitters," Nat. Photon. **3**, 658–661 (2009).

[14] A. G. Curto, G. Volpe, T. H. Taminiau, M. P. Kreuzer, R. Quidant, and N. F. van Hulst, "Unidirectional emission of a quantum dot coupled to a nanoantenna," Science **329**, 930–933 (2010).

[15] Z. Ruan, and S. Fan, "Superscattering of light from subwavelength nanostructures," Phys. Rev. Lett. **105**, 013901 (2010).

[16] N. Yu, P. Genevet, M. A. Kats, F. Aieta, J.-P. Tetienne, F. Capasso, and Z. Gaburro, "Light propagation with phase discontinuities: generalized laws of reflection and refraction," Science **334**, 333–337 (2011).

[17] C. Wu, B. Neuner III, G. Shvets, J. John, A. Milder, B. Zollars, and S. Savoy, "Large-area wide-angle spectrally selective plasmonic absorber," Phys. Rev. B **84**, 075102 (2011).

[18] R. Walter, A. Tittl, A. Berrier, F. Sterl, T. Weiss, and H. Giessen, "Large-area low-cost tunable plasmonic perfect absorber in the near infrared by colloidal etching lithography," Adv. Opt. Mater. **3**, 201400545 (2015).

[19] M. Yan, J. Dai, and M. Qiu, "Lithography-free broadband visible light absorber based on a mono-layer of gold nanoparticles," J. Opt. **16**, 025002 (2014).

[20] W. R. Holland, and D. Hall, "Frequency shifts of an electric-dipole resonance near a conducting surface," Phys. Rev. Lett. **52**, 1041–1044 (1984).

[21] J. Cesario, R. Quidant, G. Badenes, and S. Enoch, "Electromagnetic coupling between a metal nanoparticle grating and a metallic surface," Opt. Lett. **30**, 3404–3406 (2005).

[22] G. Lévêque, and O. J. F. Martin, "Optical interactions in a plasmonic particle coupled to a metallic film," Opt. Express **14**, 9971–9981 (2006).

[23] M. Yan, "Metal-insulator-metal light absorber: a continuous structure," J. Opt. **15**, 025006 (2013).

[24] P. B. Johnson, and R. W. Christy, "Optical constants of the noble metals," Phys. Rev. B **6**, 4370–4379 (1972).

[25] E. D. Palik (ed.), *Handbook of optical constants of solids* (New York, Academic Press, 1985).

[26] A. D. Rakić, "Algorithm for the determination of intrinsic optical constants of metal films: application to aluminum," Appl. Optics **34**, 4755–4767 (1995).